New Journal of Physics
The open access journal at the forefront of physics

Deutsche Physikalische Gesellschaft DPG IOP Institute of Physics

PAPER • OPEN ACCESS

An intuitive approach to structuring the three electric field components of light

To cite this article: F Maucher *et al* 2019 *New J. Phys.* **21** 013032

New Journal of Physics
The open access journal at the forefront of physics

Deutsche Physikalische Gesellschaft DPG
IOP Institute of Physics

Published in partnership with: Deutsche Physikalische Gesellschaft and the Institute of Physics

OPEN ACCESS

RECEIVED
11 November 2018

REVISED
1 December 2018

ACCEPTED FOR PUBLICATION
7 December 2018

PUBLISHED
30 January 2019

PAPER

An intuitive approach to structuring the three electric field components of light

F Maucher[1,2,3], **S Skupin**[4], **S A Gardiner**[2] **and I G Hughes**[2]

[1] Department of Physics and Astronomy, Aarhus University, Ny Munkegade 120, DK-8000 Aarhus C, Denmark
[2] Joint Quantum Centre (JQC) Durham-Newcastle, Department of Physics, Durham University, Durham DH1 3LE, United Kingdom
[3] Department of Mathematical Sciences, Durham University, Durham DH1 3LE, United Kingdom
[4] Univ. Lyon, Université Claude Bernard Lyon 1, CNRS, Institut Lumière Matière, F-69622, Villeurbanne, France

E-mail: maucher@phys.au.dk

Keywords: electromagnetic optics, laser beam shaping, optical vortices, tighly focused beams

Abstract

This paper presents intuitive interpretations of tightly focused beams of light by drawing analogies with two-dimensional electrostatics, magnetostatics and fluid dynamics. We use a Helmholtz decomposition of the transverse electric field components in the transverse plane to introduce generalized radial and azimuthal polarization states. This reveals the interplay between transverse and longitudinal electric field components in a transparent fashion. Our approach yields a comprehensive understanding of tightly focused laser beams, which we illustrate through several insightful examples.

1. Introduction

Unless the beam's transverse electric field components are divergence-free in the two-dimensional transverse plane [1], tightly focused light typically leads to a non-negligible longitudinal electric field component [2, 3], where the terms longitudinal and transverse electric field components refer to the components of the electric field that are parallel or perpendicular, respectively, to the direction of the mean Poynting flux. Having a longitudinal electric field component does not add a new degree of freedom, in the sense that all components of the electric and magnetic fields are still fixed by prescribing two components in a plane. However, it is the electric field component *parallel* to the direction of the Poynting flux, and that makes it somewhat special. Taking the longitudinal electric field component properly into account leads to a range of novel physical phenomena, such as a significant decrease of the focal spot size [4, 5], the realization of so-called 'needle beams' [6] and Möbius strips in the polarization of light [7]. In the context of light-matter interaction, taking into account the effect of the longitudinal electric field component can be crucial [8], and it may even dominate over the transverse components [9].

While the longitudinal electric field component and its interplay with the transverse components has attracted significant interest over the last two decades [3, 10, 11, 12], the discussion has usually been limited to special cases assuming certain spatial symmetries, and a simple and general intuitive picture would be highly desirable. This paper aims to provide such a picture, and presents a novel approach towards an intuitive understanding of tightly focused beams by making analogies with fluid dynamics and with two-dimensional magneto- and electrostatics. For this, a two-dimensional Helmholtz decomposition of the transverse electric field components in the transverse plane [1] is key. The Helmholtz decomposition allows the generalization of the notion of 'radial' and 'azimuthal' polarization in the following way: *radial polarization* corresponds to an electric field that is 'curl-free' in the transverse plane—which as we shall see can be interpreted as a flow solely due to sinks and sources without vorticity—and is the part of the field that gives rise to the longitudinal polarization. An *azimuthally polarized* electric field is 'divergence-free' in the transverse plane—analogous with a flow solely due to vorticity without any sinks or sources—and does not give rise to any longitudinal electric field component. Employing those polarization states turns out to be very useful for computing numerically exact solutions to Maxwell's equations with structured electric field components, and moreover facilitates an intuitive understanding of tightly focused vector beams.

The paper is organized as follows. In section 2 we introduce the nomenclature, present the equations of motion, and detail the connection between radially and azimuthally polarized fields, and curl- and divergence-free solutions in the transverse plane. In section 3 we draw analogies with electrostatics, magnetostatics and fluid dynamics, hence presenting intuitive interpretations of fields that are 'divergence-free' and 'curl-free' in the transverse plane. Finally, in section 4 we present several intuitive examples to illustrate the analogies and convey an appreciation of the concept of generalized radial and azimuthal polarization states. Starting with basic Laguerre–Gaussian (LG) modes, we show constructions of complex random and topological beams.

2. Model

The three electric field components of a tightly focused monochromatic beam (frequency ω, wavelength $\lambda = 2\pi c/\omega$, vacuum light velocity c) in free space are described by

$$\nabla^2 \mathbf{E}(\mathbf{r}_\perp, z) + k_0^2 \mathbf{E}(\mathbf{r}_\perp, z) = 0, \tag{1}$$

$$\nabla \cdot \mathbf{E}(\mathbf{r}_\perp, z) = \nabla_\perp \cdot \mathbf{E}_\perp + \partial_z E_z = 0. \tag{2}$$

We have introduced $k_0^2 = \omega^2/c^2 = (2\pi/\lambda)^2$, the transverse coordinates $\mathbf{r}_\perp = (x, y)$, and the transverse electric field components $\mathbf{E}_\perp = (E_x, E_y)$. In what follows, we consider the wavelength λ to be a fixed scaling parameter to equation (1). Note that $\mathbf{E}$ represents the complex amplitude vector of the beam; the full electric field has an additional trivial time-dependence $\exp(-\mathrm{i}\omega t)$ that is omitted here.

For a given amplitude vector in the focal plane[5] $\mathbf{E}^{\mathrm{f}}(\mathbf{r}_\perp) = \mathbf{E}(\mathbf{r}_\perp, z = 0)$, the propagation in the positive z direction can be easily computed in the transverse spatial Fourier domain as

$$\hat{\mathbf{E}}(\mathbf{k}_\perp, z) = \hat{\mathbf{E}}^{\mathrm{f}}(\mathbf{k}_\perp) \mathrm{e}^{\mathrm{i}k_z(\mathbf{k}_\perp)z}, \tag{3}$$

where $k_z(\mathbf{k}_\perp) = \sqrt{k_0^2 - \mathbf{k}_\perp^2}$ and $\mathbf{k}_\perp = (k_x, k_y)$; the symbol $\hat{}$ denotes the Fourier transform with respect to $\mathbf{r}_\perp$. It is important to note that $\mathbf{E}^{\mathrm{f}}$ cannot be arbitrarily prescribed in all three components. We use a two-dimensional Helmholtz decomposition to depict the most general expression for the two transverse components, as [1]

$$\mathbf{E}_\perp^{\mathrm{f}}(\mathbf{r}_\perp) = -\begin{pmatrix} \partial_x V(\mathbf{r}_\perp) \\ \partial_y V(\mathbf{r}_\perp) \end{pmatrix} + \begin{pmatrix} 0 & 1 \\ -1 & 0 \end{pmatrix} \begin{pmatrix} \partial_x W(\mathbf{r}_\perp) \\ \partial_y W(\mathbf{r}_\perp) \end{pmatrix}, \tag{4}$$

where $V(\boldsymbol{r}_\perp)$ and $W(\boldsymbol{r}_\perp)$ denote arbitrary (sufficiently well behaved) scalar potentials. The first term, which we denote $\mathbf{E}_\perp^{\mathrm{f},V} = -\nabla_\perp V$, corresponds to a field that is curl-free in the transverse two-dimensional plane, that is, $\nabla_\perp \times \mathbf{E}_\perp^{\mathrm{f},V} = 0$. The second term we denote $\mathbf{E}_\perp^{\mathrm{f},W} = (\partial_y W, -\partial_x W)$, which gives rise to a divergence-free field in the transverse two-dimensional plane,[6] that is, $\nabla_\perp \cdot \mathbf{E}_\perp^{\mathrm{f},W} = 0$. The longitudinal electric field component E_z is therefore coupled solely to $\mathbf{E}_\perp^{\mathrm{f},V}$, and together with the potential V it obeys a Poisson equation

$$\Delta_\perp V(\mathbf{r}_\perp) = \partial_z E_z|_{z=0}(\mathbf{r}_\perp). \tag{5}$$

Because the z dependence of E_z is known from equation (3), E_z^{f} can be readily obtained in Fourier space from

$$-\mathbf{k}_\perp^2 \hat{V}(\mathbf{k}_\perp) = \mathrm{i}k_z(\mathbf{k}_\perp) \hat{E}_z^{\mathrm{f}}(\mathbf{k}_\perp). \tag{6}$$

For given potentials V and W the full solution can therefore be written in transverse Fourier space as

$$\hat{\mathbf{E}}(\mathbf{k}_\perp, z) = \mathrm{i}\left[\begin{pmatrix} -k_x \\ -k_y \\ \dfrac{\mathbf{k}_\perp^2}{k_z(\mathbf{k}_\perp)} \end{pmatrix} \hat{V}(\mathbf{k}_\perp) + \begin{pmatrix} k_y \\ -k_x \\ 0 \end{pmatrix} \hat{W}(\mathbf{k}_\perp) \right] \mathrm{e}^{\mathrm{i}k_z(\mathbf{k}_\perp)z}. \tag{7}$$

Hence, the potential V generates the electric field $\mathbf{E}^V$, the three vector components of which are in general nonzero. By way of contrast, the potential W generates the electric field $\mathbf{E}^W$, the longitudinal component of which vanishes ($E_z^W = 0$). For reasons which become clear in section 4.1 we will call $\mathbf{E}^V$ *radially polarized*, and $\mathbf{E}^W$ *azimuthally polarized*. Other polarization states imply certain conditions on the potentials V and W: *transverse linear polarization*, with $\alpha E_x = (1 - \alpha) E_y$ with $0 \leqslant \alpha \leqslant 1$, requires

$$[\alpha k_x - (1 - \alpha) k_y] \hat{V}(\mathbf{k}_\perp) = [\alpha k_y + (1 - \alpha) k_x] \hat{W}(\mathbf{k}_\perp); \tag{8}$$

[5] Any other $z =$ constant plane could also be used.

[6] The electric field in vacuum always fulfills $\nabla \cdot \mathbf{E} = 0$. Hence, the restriction 'in the transverse two-dimensional plane' is crucial in the present context.

Table 1. Analogy with electrostatics in two dimensions.

	Electrostatics (2D)	$W = 0$ solutions
Charge:	$\rho(x, y)$	$-\partial_z E_z\vert_{z=0}$
Curl-free:	$\nabla_\perp \times \mathbf{E}^{\mathrm{s}}_\perp = 0$	$\nabla_\perp \times \mathbf{E}^{\mathrm{f},V}_\perp = 0$
Field:	$\mathbf{E}^{\mathrm{s}}_\perp = -\nabla_\perp \phi$	$\mathbf{E}^{\mathrm{f},V}_\perp = -\nabla_\perp V$
Poisson-eq.:	$\Delta_\perp \phi = -\rho(x, y)$	$\Delta_\perp V = \partial_z E_z\vert_{z=0}$

and *transverse circular polarization*, with $E_x = \pm\, \mathrm{i}E_y$, requires

$$\hat{V}(\mathbf{k}_\perp) = \pm \mathrm{i}\hat{W}(\mathbf{k}_\perp). \tag{9}$$

These definitions do not involve the longitudinal component E_z, which is why they are termed *transverse*. From equations (8) and (9), the well-known fact that any nonzero linearly or circularly polarized field necessarily gives rise to a longitudinal electric field component becomes immediately clear; in these cases V is nonzero and has a nontrivial spatial dependence, and hence equation (5) gives rise to a nonzero E_z. Throughout this paper, we will refer to these transverse polarization states when we mention linear and circular polarization. We note, however, that in the definitions for linear and circular polarization involving all three electric field components (see, e.g. [11]) both cases would be elliptically polarized.

Before we consider analogies and interpretations of the expressions found, we would like to connect our approach to the respective literature. The generating potentials for tightly focused vector beams were formulated in [11, 13]: given a scalar solution Ψ to the scalar Helmholtz equation, we can write down the transverse magnetic polarized field (TM polarization) as $\mathbf{B} \propto (\partial_y \Psi,\ -\partial_x \Psi,\ 0)$, and the associated electric field reads $\mathbf{E} \propto (\partial_x \partial_z \Psi,\ \partial_y \partial_z \Psi,\ -\partial_x^2 \Psi - \partial_y^2 \Psi)$. Hence, a TM beam corresponds to a field $\mathbf{E}^V$ with $V \propto \partial_z \Psi$ in our nomenclature. The transverse electric polarized field (TE polarization) can be readily obtained via the dual transformation $\mathbf{E} \to c\mathbf{B}$ and $\mathbf{B} \to -\mathbf{E}/c$, corresponding to a field $\mathbf{E}^W$ with $W \propto \Psi$ in our nomenclature. However, the notations TM and TE polarization are usually used in the context of two-dimensional systems with translational invariance in one direction (Fresnel reflection, waveguides, etc.), and thus we do not adopt them here. Moreover, this paper focuses primarily on the electric field $\mathbf{E}$ and henceforth we will not discuss the magnetic field $\mathbf{B}$. An experimental visualization of the structures presented in this work would entail some form of atom-light interactions, and it is well known that the electric field dominates the magnetic field when interacting with charges in a medium (see, e.g. [14]).

3. Interpretations and analogies

Let us now interpret the equations from the last section and lay out analogies with two-dimensional electro- and magnetostatics and fluid dynamics.

3.1. Curl-free fields produced by potential V

We first consider fields $\mathbf{E}^V$ that are curl-free in the transverse plane, that is, fields obtained when $W = 0$. The aim is to understand how the transverse electric field components $\mathbf{E}^{\mathrm{f},V}_\perp$ relate to the longitudinal component E^{f}_z. Equation (5) represents a Poisson equation in two dimensions for the potential $V(x, y)$, the solution of which in transverse Fourier space is given by equation (6). The source term for this Poisson equation is given by $\partial_z E_z\vert_{z=0}$, which depends on the transverse coordinates $\mathbf{r}_\perp$ only.

The source term $\partial_z E_z\vert_{z=0}$ involves the longitudinal derivative, and not the component E^{f}_z directly. However, making use of equation (3) in transverse Fourier space we can approximate the source term to lowest order as

$$\partial_z \hat{E}_z\vert_{z=0}(\mathbf{k}_\perp) = \mathrm{i}k_z(\mathbf{k}_\perp)\hat{E}^{\mathrm{f}}_z(\mathbf{k}_\perp) \approx \mathrm{i}k_0 \hat{E}^{\mathrm{f}}_z(\mathbf{k}_\perp) + \mathcal{O}\left(\frac{\mathbf{k}_\perp^2}{k_0^2}\right), \tag{10}$$

thereby disposing of this derivative term. Equation (10) is of course only a rough estimate, with an error that grows with the degree of the light's non-paraxiality. It nevertheless gives an idea of the qualitative behavior of E^{f}_z, as will be illustrated in section 4.

To see the analogy with two-dimensional electrostatics, we must simply identify $-\partial_z E_z\vert_{z=0}$ with a charge density $\rho(x, y)$. The transverse electric field components $\mathbf{E}^{\mathrm{f},V}_\perp$ then follow from the same equations as the two-dimensional electrostatic field $\mathbf{E}^{\mathrm{s}}_\perp(x,\ y)$, as summarized in table 1.

There is, however, a subtlety related to this analogy requiring comment. The optical field amplitude $\mathbf{E}$ is complex-valued, and the full electric field has a temporal dependence that is hidden in this representation, unlike the two-dimensional electrostatic field which is real-valued and time-independent. Thus, in general, we must separate the real and imaginary parts of $\mathbf{E}$ and solve two 'electrostatic' problems.

Table 2. Analogy with magnetostatics in two dimensions.

Magnetostatics with $\boldsymbol{J}^{\mathrm{s}} = J_z^{\mathrm{s}}(\mathbf{r}_\perp)\boldsymbol{e}_z$		$V = 0$ solutions
Current:	$\mu_0 J_z^{\mathrm{s}} = \partial_x B_y^{\mathrm{s}} - \partial_y B_x^{\mathrm{s}}$	$\partial_x E_y^{\mathrm{f}} - \partial_y E_x^{\mathrm{f}}$
Div.-free:	$\nabla_\perp \cdot \mathbf{B}_\perp^{\mathrm{s}} = 0$	$\nabla_\perp \cdot \mathbf{E}_\perp^{\mathrm{f},W} = 0$
Field:	$\mathbf{B}_\perp^{\mathrm{s}} = (\partial_y A_z^{\mathrm{s}}, -\partial_x A_z^{\mathrm{s}})$	$\mathbf{E}_\perp^{\mathrm{f},W} = (\partial_y W, -\partial_x W)$
Poisson-eq.:	$\Delta_\perp A_z^{\mathrm{s}} = -\mu_0 J_z^{\mathrm{s}}$	$\Delta_\perp W = \partial_y E_x^{\mathrm{f}} - \partial_x E_y^{\mathrm{f}}$

3.2. Divergence-free fields produced by potential W

Here we are interested in solutions $\mathbf{E}^W$ that are divergence-free in the transverse plane ($V = 0$, and consequently $E_z^W = 0$). The potential W can be interpreted as the longitudinal component of a vector potential, that is, $\mathbf{E}^{\mathrm{f},W} = \nabla \times W\boldsymbol{e}_z$. Then, by taking the curl of this equation, we get

$$\Delta_\perp W(\mathbf{r}_\perp) = \partial_y E_x^{\mathrm{f}}(\mathbf{r}_\perp) - \partial_x E_y^{\mathrm{f}}(\mathbf{r}_\perp), \tag{11}$$

a Poisson equation for the potential W.

This leads to a straightforward analogy with *magnetostatics*[7]. If we identify the potential W with the only nonzero component A_z^{s} of a magnetic vector potential

$$\boldsymbol{A}^{\mathrm{s}}(\mathbf{r}_\perp) = A_z^{\mathrm{s}}(\mathbf{r}_\perp)\boldsymbol{e}_z, \tag{12}$$

the induced static magnetic field $\boldsymbol{B}^{\mathrm{s}} = \nabla \times \boldsymbol{A}^{\mathrm{s}}$ can be associated with $\boldsymbol{E}^{\mathrm{f},W}$. The static current density follows from $\nabla \times \boldsymbol{B}^{\mathrm{s}} = \mu_0 \boldsymbol{J}^{\mathrm{s}}$, and flows perpendicular to the (x,y) plane under consideration. Hence, J_z^{s} is the only nonzero component, and corresponds to the negative source term in equation (11). The complete magnetostatic analogy is summarized in table 2.

A similar remark as given above concerning the complex-valued optical field amplitude applies, in that two real-valued magnetostatic problems may need to be solved to describe one curl-free optical field. Furthermore, it is important to note that this represents a formal analogy only; the analog magnetic field $\mathbf{B}^{\mathrm{s}}$ must not be confused with the magnetic field $\mathbf{B}$ of the vector beam (see also the discussion at the very end of section 2).

3.3. Fields produced by both potentials V and W

In the most general situation, both potentials V and W are nonzero. In this case the optical field $\boldsymbol{E}^{\mathrm{f}} = \boldsymbol{E}^{\mathrm{f},V} + \boldsymbol{E}^{\mathrm{f},W}$ has a perfect analogy in fluid dynamics [15]. For a fluid with density ϱ and flow velocity field $\mathbf{u}$, conservation of mass dictates the continuity equation

$$\partial_t \varrho(\mathbf{r}, t) + \nabla \cdot [\varrho(\mathbf{r}, t)\mathbf{u}(\mathbf{r}, t)] = 0. \tag{13}$$

We consider a layer of this fluid in a $z =$ constant plane, e.g. $z = 0$, with in- and outflow ϱu_z into the layer. We denote the flow velocity field in this layer $\mathbf{u}^{\mathrm{l}}(\mathbf{r}_\perp) = \mathbf{u}(\mathbf{r}_\perp, z = 0)$. In the stationary situation ($\partial_t \varrho = 0$), and furthermore assuming homogenity and incompressibility ($\nabla \varrho = 0$), we find that

$$\nabla_\perp \cdot \mathbf{u}_\perp^{\mathrm{l}}(\mathbf{r}_\perp) = -\partial_z u_z|_{z=0}(\mathbf{r}_\perp). \tag{14}$$

Equation (14) is identical to equation (2) if we identify $\mathbf{u}_\perp^{\mathrm{l}}$ with $\boldsymbol{E}_\perp^{\mathrm{f}}$, and we write $\mathbf{u}_\perp^{\mathrm{l}} = \mathbf{u}_\perp^{\mathrm{l,cf}} + \mathbf{u}_\perp^{\mathrm{l,df}}$, where $\mathbf{u}_\perp^{\mathrm{l,cf}}$ is curl-free in the $z = 0$ plane ($\nabla_\perp \times \mathbf{u}_\perp^{\mathrm{l,cf}} = 0$), and $\mathbf{u}_\perp^{\mathrm{l,df}}$ divergence-free ($\nabla_\perp \cdot \mathbf{u}_\perp^{\mathrm{l,df}} = 0$).

The analogy between $\mathbf{u}_\perp^{\mathrm{l,cf}}$ and $\boldsymbol{E}^{\mathrm{f},V}$ follows immediately: the curl-free velocity field $\mathbf{u}_\perp^{\mathrm{l,cf}}$ can be written as the negative gradient of the so-called velocity potential ϕ, and the spatial in- and outflow rate $\partial_z u_z|_{z=0}$ acts as a source term in the Poisson equation for the velocity potential, as shown in table 3.

Following [15], let us now turn towards the divergence-free (two-dimensional) velocity field $\mathbf{u}_\perp^{\mathrm{l,df}}$, which obeys the continuity equation

$$\partial_x u_x^{\mathrm{l,df}}(\mathbf{r}_\perp) + \partial_y u_y^{\mathrm{l,df}}(\mathbf{r}_\perp) = 0. \tag{15}$$

This implies that the differential $\mathrm{d}\psi = u_x^{\mathrm{l,df}}\mathrm{d}y - u_y^{\mathrm{l,df}}\mathrm{d}x$ is exact, and the scalar *stream function* ψ can be found (up to a constant) as line integral from some reference point $\mathcal{O}$ to a given point $\mathcal{P}$

$$\psi(\mathcal{P}) - \psi(\mathcal{O}) = \int_{\mathcal{O}}^{\mathcal{P}} \mathrm{d}\psi = \int_{\mathcal{O}}^{\mathcal{P}} u_x^{\mathrm{l,df}}\mathrm{d}y - u_y^{\mathrm{l,df}}\mathrm{d}x. \tag{16}$$

In particular any integration curve joining the two points yields the same result[8]. In fluid dynamics, the stream function characterizes the flow velocity quite intuitively, as already suggested by its name. The 'flux' across a

[7] We follow the common terminology which labels magnetic fields of stationary currents as *magnetostatic*, even though time inversion symmetry is violated.

[8] We consider a simply connected region.

Table 3. Analogy with curl-free velocity field flow.

Fluid dynamics (2D)		$W = 0$ solutions
Sources and sinks:	$\partial_z u_z\|_{z=0}$	$\partial_z E_z\|_{z=0}$
Curl-free:	$\nabla_\perp \times \mathbf{u}_\perp^{\mathrm{l,cf}} = 0$	$\nabla_\perp \times \mathbf{E}_\perp^{\mathrm{f,}\,V} = 0$
Field:	$\mathbf{u}_\perp^{\mathrm{l,cf}} = -\nabla_\perp \phi$	$\mathbf{E}_\perp^{\mathrm{f,}\,V} = -\nabla_\perp V$
Poisson-eq.:	$\Delta_\perp \phi = \partial_z u_z\|_{z=0}$	$\Delta_\perp V = \partial_z E_z\|_{z=0}$

Table 4. Analogy with divergence-free velocity field flow.

Fluid dynamics (2D)		$V = 0$ solutions
Vorticity:	$\Omega = \partial_x u_y^{\mathrm{l}} - \partial_y u_x^{\mathrm{l}}$	$\partial_x E_y^{\mathrm{f}} - \partial_y E_x^{\mathrm{f}}$
Div.-free:	$\nabla_\perp \cdot \mathbf{u}_\perp^{\mathrm{l,df}} = 0$	$\nabla_\perp \cdot \mathbf{E}_\perp^{\mathrm{f},W} = 0$
Field:	$\mathbf{u}_\perp^{\mathrm{l,df}} = (\partial_y \psi, -\partial_x \psi)$	$\mathbf{E}_\perp^{\mathrm{f},W} = (\partial_y W, -\partial_x W)$
Poisson-eq.:	$\Delta \psi = -\Omega$	$\Delta W = \partial_y E_x^{\mathrm{f}} - \partial_x E_y^{\mathrm{f}}$

closed curve, that is, $\mathcal{P} = \mathcal{O}$, is zero. Since the 'flux' across any curve joining the two points $\mathcal{P}$ and $\mathcal{O}$ depends only on the values of ψ at these two points, it is clear that ψ is constant along a streamline.

In fluid dynamics, one commonly defines the *vorticity* as

$$\boldsymbol{\omega} = \nabla \times \mathbf{u}_\perp^{\mathrm{l}} = (\partial_x u_y^{\mathrm{l}} - \partial_y u_x^{\mathrm{l}})\boldsymbol{e}_z = \Omega \boldsymbol{e}_z. \tag{17}$$

The vorticity vector is oriented perpendicular to our plane of interest, and its nonzero component Ω, together with the stream function ψ, obeys a Poisson equation:

$$\Delta_\perp \psi(\mathbf{r}_\perp) = -\Omega(\mathbf{r}_\perp). \tag{18}$$

Hence, $\boldsymbol{E}_\perp^{\mathrm{f},W}$ can be interpreted as the divergence-free velocity field $\mathbf{u}_\perp^{\mathrm{l,df}}$ of a two-dimensional incompressible fluid, which is composed of vortices only and does not contain sources or sinks. The potential W must be associated with the fluid stream function ψ determined by the longitudinal component Ω of the *vorticity* $\boldsymbol{\omega}$. The full analogy is summarized in table 4.

In summary, we note that two-dimensional incompressible fluid dynamics permits coverage of the cases of both curl- and divergence-free fields ($V = 0$ and $W = 0$, respectively), as shown in tables 3 and 4, and thus represents a unified analogy. One must bear in mind, however, that in fluid dynamics the flow velocity field $\mathbf{u}$ is real valued, and so in general two fluid problems are necessary to represent one complex optical field.

4. Examples

We now present several intuitive examples to illustrate our findings, highlighting the concept of generalized radial and azimuthal polarization, and exploiting the aforementioned analogies to construct numerically exact vector beams.

There are two general remarks to be made before prescribing any potential or field components. Firstly, the relevant quantities must not contain any evanescent amplitudes, that is, in the transverse Fourier domain $\mathbf{k}_\perp$ all fields and potentials must be zero for $\mathbf{k}_\perp^2 \geqslant k_0^2$. Otherwise, equation (3) gives an exponentially growing solution for negative z, which renders it unphysical in the bulk. Therefore, in the examples that follow we systematically apply the filter function

$$H_{k_0}(\boldsymbol{k}_\perp) = \begin{cases} \exp\left[-\dfrac{1}{2\lambda^2(\sqrt{\boldsymbol{k}_\perp^2} - k_0)^2}\right] & \text{for } \boldsymbol{k}_\perp^2 < k_0^2 \\ 0 & \text{for } \boldsymbol{k}_\perp^2 \geqslant k_0^2 \end{cases} \tag{19}$$

to these quantities. Secondly, equation (2) implies that $\hat{E}_z^{\mathrm{f}}(\mathbf{k}_\perp = 0) = 0$ for solutions propagating in the z direction. This is automatically fulfilled when E_z^{f} (or $\partial_z E_z|_{z=0}$) is computed from a given potential V. However, if E_z^{f} (or $\partial_z E_z|_{z=0}$) is prescribed, special care must be taken. A suitable filter function is then

$$H_0(\boldsymbol{k}_\perp) = 1 - \mathrm{e}^{-(3\lambda \boldsymbol{k}_\perp)^2}, \tag{20}$$

which we have applied in the examples below when needed.

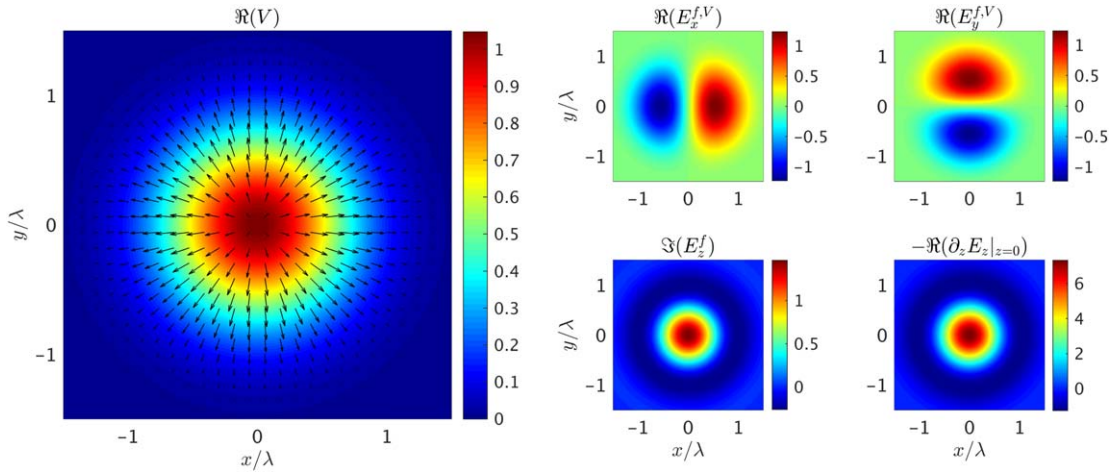

Figure 1. A real-valued Gaussian potential $V \propto \exp(-2\boldsymbol{r}_\perp^2/\lambda^2)$ produces a radially polarized beam. The transverse electric field $\boldsymbol{E}_\perp^{\mathrm{f},V}$ is indicated by arrows. The induced field components and the 'charge density' $-\partial_z E_z|_{z=0}$ are shown on the right.

4.1. Radial and azimuthal polarization

Let us first consider the simplest examples of bell-shaped V and W potentials, producing classic radially and azimuthally polarized vector beams, respectively. In terms of LG profiles, we therefore take $\mathrm{LG}_{00}^{\sigma}(\mathbf{r}_\perp)$, that is, a simple Gaussian, fixing its width to $\sigma = \lambda/2$. As explained above, we must filter the potentials in the transverse Fourier domain by multiplying them by H_{k_0} in order to remove evanescent waves.

4.1.1. Gaussian 'electrostatic potential' V

Given that we use the constraint $W = 0$, and V is chosen to be a real-valued function, we require only the real parts of $\boldsymbol{E}_\perp^{\mathrm{f},V}$ and $\partial_z E_z|_{z=0}$, and the imaginary part of E_z^{f}. We therefore depict these components only in figure 1, which displays the resulting radially polarized beam. It follows straightforwardly that we get two dipole-like light distributions in the transverse electric field components from such a bell-shaped 'electrostatic potential' V. Going further with this analogy, the 'charge density' $-\partial_z E_z|_{z=0} \propto (1 - 2\boldsymbol{r}_\perp^2/\lambda^2)\exp(-2\boldsymbol{r}_\perp^2/\lambda^2)$ inducing such a potential consists of a positive hump and a negative ring. The shape of this 'charge density' is very close to the longitudinal component E_z^{f}, which justifies the estimation given by equation (10).

4.1.2. Gaussian 'magnetic vector potential' W

In order to produce an azimuthally polarized vector beam, we simply let W be the real-valued Gaussian, and set $V = 0$. Figure 2 shows that the vector field $\mathbf{E}_\perp^{\mathrm{f},W}$ is tangential to the contour lines of W. This is exactly what one would expect from the magnetostatic analogy, where W corresponds to the longitudinal component A_z^{s} of the magnetic vector potential. We do not depict the static current density J_z^{s} that would generate such a vector potential and respective magnetostatic field. However, its profile has exactly the same form as the 'charge density' $-\partial_z E_z|_{z=0}$ in figure 1: a positive bell-shaped current density at the center, surrounded by a negative ring-like return current.

4.1.3. Circularly polarized vortex beam

In section 2, we discussed how to choose the potentials V and W such that the transverse fields are circularly polarized, namely $\pm \mathrm{i}W = V$. Hence, complex superposition of the fields shown in figures 1 and 2 should give a circularly polarized beam. In figure 3 we display the resulting transverse field components E_x^{f} and E_y^{f}, which are indeed two singly charged vortices. The corresponding longitudinal electric field component E_z^{f} is not shown, because it is the same as that shown in figure 1.

This rather straightforward construction of circularly polarized beams works for any pair of generalized radially and azimuthally polarized beams with $\pm \mathrm{i}W = V$. The motivation for this consideration stems from the fact that in such an arrangement one has a beam that is both linearly (the longitudinal electric field component) as well as circularly polarized (the transverse polarization components). This could play an important role for imprinting structures onto matter, since the longitudinal electric field component could drive a different transition to the transverse electric field components.

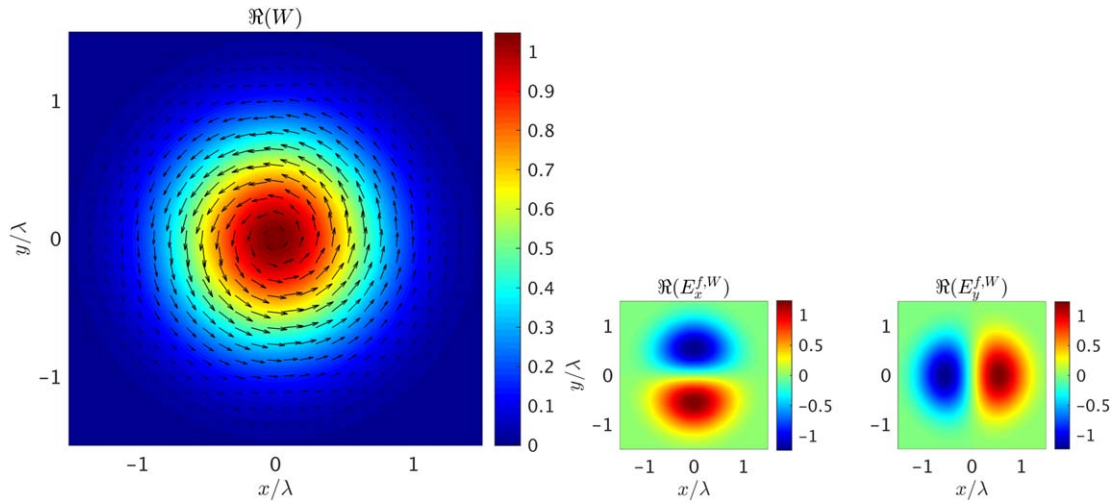

Figure 2. A real-valued Gaussian potential $W \propto \exp(-2\boldsymbol{r}_\perp^2/\lambda^2)$ produces an azimuthally polarized beam. The purely transverse electric field $\boldsymbol{E}_\perp^{f,W}$ is indicated by arrows. The induced field components are shown on the right ($E_z^f = 0$).

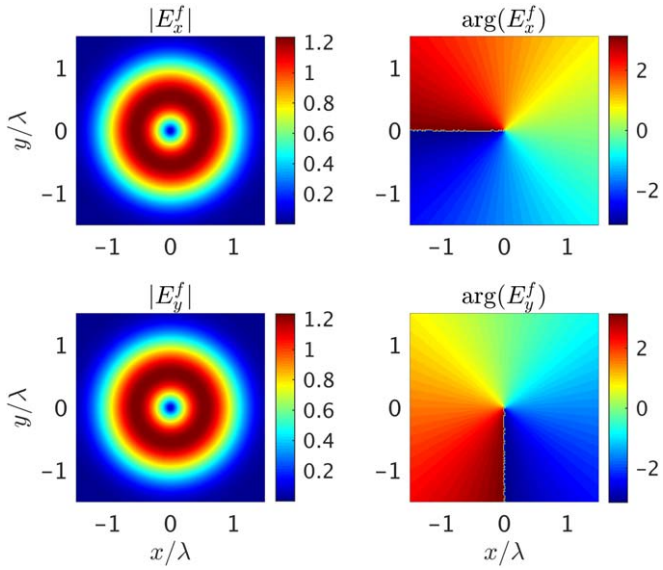

Figure 3. Transverse field components of a circularly polarized single charge vortex beam produced by complex superposition of figures 1 and 2, that is, $V = \mathrm{i}W \propto \exp(-2\boldsymbol{r}_\perp^2/\lambda^2)$.

4.2. Longitudinal vortex beam

Let us now use our previous findings to construct a beam featuring a singly charged vortex in its longitudinal component E_z^f. Because such a vortex is composed of two orthogonal dipoles in the real and imaginary parts, we may start with a dipole. Moreover, we want to make use of the fluid dynamics analogy, and prescribe a real-valued dipole in the 'spatial in- and outflow rate,' $\partial_z E_z|_{z=0} \propto x \exp(-2\boldsymbol{r}_\perp^2/\lambda^2)$. The induced velocity potential is easily obtained in the transverse Fourier domain as

$$\hat{\phi}^{\mathrm{dipole}} \propto H_{k_0} k_x \exp(-\lambda^2 \boldsymbol{k}_\perp^2/8)/\boldsymbol{k}_\perp^2, \tag{21}$$

where we apply the filter function H_{k_0} to remove any evanescent waves. The resulting potential in position space is shown in figure 4, together with all electric field components. In terms of the fluid dynamics analogy, where we interpret the transverse field as the flow velocity, a very intuitive picture arises: peak and trough of the dipole in $\partial_z E_z|_{z=0}$ act like source and sink for the 'flow.' With the approximation equation (10), even the longitudinal component E_z^f by itself can be identified with the source of the 'transverse flow.'

In principle, we can now construct a beam with the desired singly charged vortex in its longitudinal component by employing the potential $V(x, y) = \phi^{\mathrm{dipole}}(x, y) \pm \mathrm{i}\phi^{\mathrm{dipole}}(y, x)$, that is, by adding ϕ^{dipole} rotated by $\pm\pi/2$ as the imaginary part of V. The resulting beam is radially polarized in the generalized sense

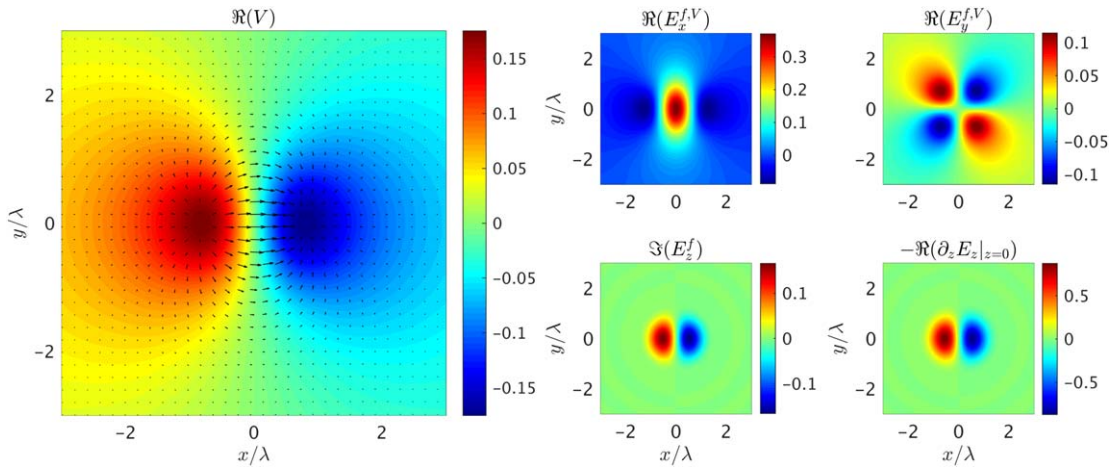

Figure 4. A real-valued dipole is prescribed in $\partial_z E_z|_{z=0}$, and the resulting potential $V = \phi^{\text{dipole}}$ (see text for details) is used to compute the electric field components.

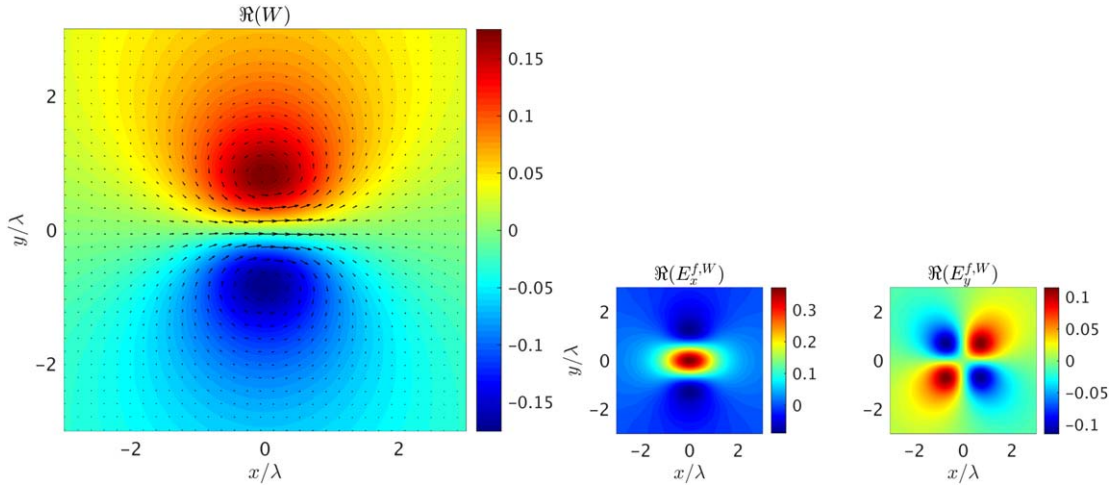

Figure 5. The real-valued potential $W(x, y) = -\phi^{\text{dipole}}(y, x)$ (see text for details) produces $E_y^{\text{f},W} = -E_y^{\text{f},V}$ of figure 4.

introduced earlier, because $W = 0$. It is, however, not the easiest realization of a longitudinal vortex, as we will see below.

The transverse electric field components $E_x^{\text{f},V}$ and $E_y^{\text{f},V}$ shown in figure 4 appear to be relatively intricate, and so the natural question arises whether it is possible to simplify the 'transverse flow' by adding a divergence-free velocity field through an appropriate stream function ψ. The main flow is clearly in the positive x direction, and so we may choose the stream function ψ such that the y component of the total flow velocity is zero. Equation (8) tells us that $\hat{\psi} = -k_y \hat{\phi}^{\text{dipole}}/k_x$ will suffice, which translates into $\psi(x, y) = -\phi^{\text{dipole}}(y, x)$ in position space. And indeed, figure 5 confirms that $E_y^{\text{f},W} = -E_y^{\text{f},V}$, that is, the total 'transverse flow' is parallel to $\boldsymbol{e}_x$.

Hence, the potentials $V(x, y) = \phi^{\text{dipole}}(x, y) \pm \mathrm{i}\phi^{\text{dipole}}(y, x)$ and $W(x, y) = -\phi^{\text{dipole}}(y, x) \pm \mathrm{i}\phi^{\text{dipole}}(x, y)$ produce a longitudinal vortex as well, but with much simpler transverse field components. Figure 6 shows the resulting optical fields (for the + sign), and it even turns out that transverse components are bell-shaped. Moreover, the transverse field is circularly polarized, as $W = \mathrm{i}V$. We have therefore constructed the solution reported in [16], where a longitudinal vortex was achieved by tightly focusing a circularly polarized bell-shaped light distribution.

It is important to note that the choice of the 'stream function' W is the degree of freedom one has when only the longitudinal electric field component is prescribed. In the present example, we used W to simplify the transverse electric field components. In section 4.4, we will demonstrate that W can be used as well to engineer certain topological properties of the transverse fields.

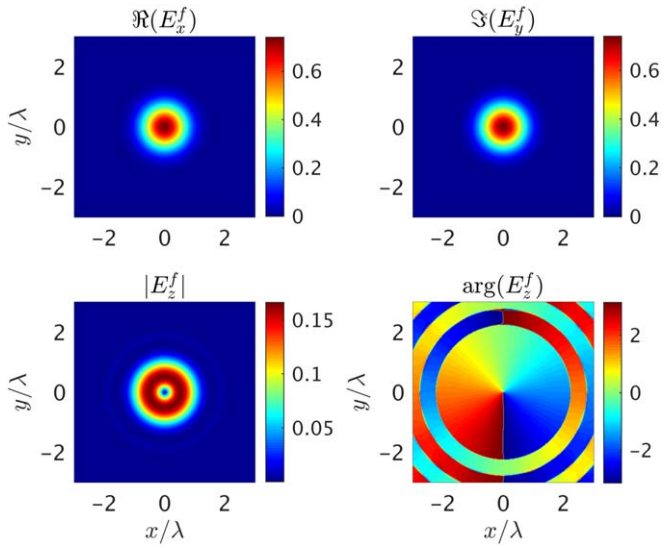

Figure 6. A bell-shaped circularly polarized transverse field produces a singly charged vortex in E_z^{f}. The off-axis sign flips in the phase plot are due to the filter function H_{k_0} (see text).

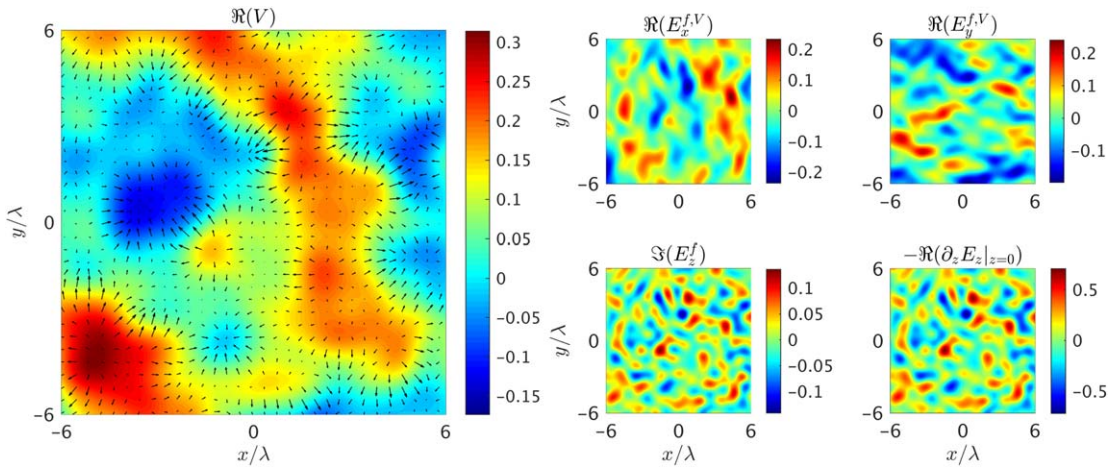

Figure 7. A random profile is prescribed in $\Im(E_z^{\mathrm{f}})$ (see text for details). The real-valued 'charge density' $-\partial_z E_z|_{z=0}$ looks very similar. Corresponding potential V and transverse field components are shown as well.

4.3. Random beam

Let us prescribe a rather complicated longitudinal field component E_z^{f}—a random beam, as shown in figure 7. For this case, we simply consider a super-Gaussian beam profile in E_z^{f}, $\exp(-r^{10}/(10\lambda)^{10})$, and multiply the latter with complex random numbers at each point of the numerical grid. The complex-valued random numbers are constructed as $f = \xi_1 \exp(2\pi \mathrm{i} \xi_2)$, with real-valued random numbers $\xi_{1,2} \in [0,\ 1]$. The resulting beam profile is then multiplied in transverse Fourier space by both filter functions H_{k_0} and H_0, as introduced above. In order to facilitate comparison with previous figures, we choose to show $\Im(E_z^{\mathrm{f}})$, such that all other derived quantities in figure 7 are real valued. Furthermore, we plot only the center part of the beam.

We now make several important remarks regarding figure 7. First of all, the 'charge density' $-\partial_z E_z|_{z=0}$, to once more take the electrostatic analogy, features a pattern very close to that prescribed in $\Im(E_z^{\mathrm{f}})$. This means that even here the approximation equation (10) yields insight, and the longitudinal component E_z^{f} can be identified directly as a 'charge density.' Moreover, figure 7 shows very nicely how the landscape of the 'electrostatic potential' $\Re(V)$ induced by $\Im(E_z^{\mathrm{f}})$ 'shapes' the transverse electric field components $\Re(\mathbf{E}_\perp^{\mathrm{f,V}})$. In contrast to the previous examples, the peaks and troughs of $\Im(E_z^{\mathrm{f}})$ cannot be directly related to the peaks and troughs of $\Re(V)$. This can be understood by thinking of V as being a convolution between the Green's function of the two-dimensional Poisson equation (which is long-ranged) and the 'charge density': the convolution

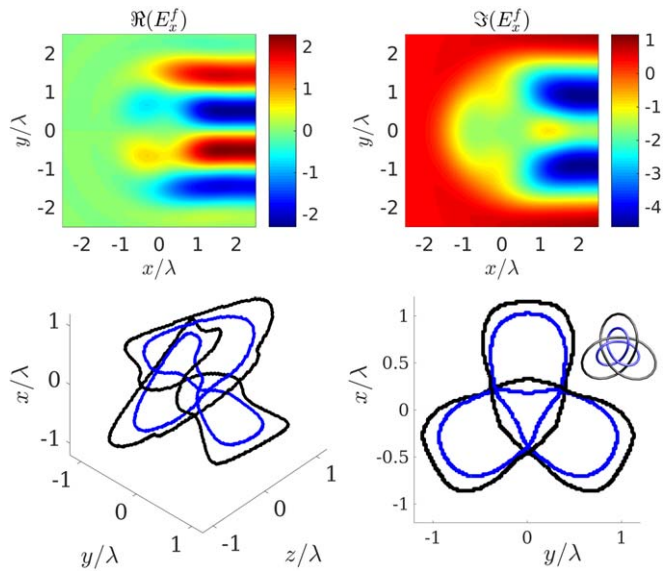

Figure 8. Two linked trefoils in different components of the electric field: the blue line represents the vortex line in E_y, the black line the vortex line in E_z. The corresponding (semi-infinite) profiles in E_x^f are shown in the upper panels.

cannot resolve the delicate structure of the source term and simply smears it out. This also explains why the structures in the transverse field components are larger than those in E_z^f.

4.4. Linked trefoils in transverse and longitudinal components

We discussed the remaining degrees of freedom when fixing the longitudinal electric field component E_z^f in section 4.2, where they were exploited to simplify the transverse profiles. In principle, nothing prevents us from prescribing two field components, say E_z^f and E_y^f, in the focal plane. This allows us to engineer both transverse and longitudinal components, and the potentials V and W determine the complete optical field via equation (7).

Here, we will demonstrate the tremendous possibilities of creating customized vector beams by creating knotted vortex lines in the longitudinal and one transverse electric field component (E_y). Apart from optics, knotted and linked vortex lines have also recently been studied in a range of different contexts, such as classical fluid dynamics [17], excitable media [18–21], nematic colloids [22–24] and superfluids such as Bose–Einstein condensates [25, 26]. In the present context, optical vortex knots [1, 27, 28] can be used to imprint topological light structures onto the latter [29, 30].

The topology of the two knots we envisage is sketched in figure 8: the vortex lines of the E_y and E_z components form two linked trefoil knots. To create such a vector beam, the respective components can be prescribed in the focal plane as

$$E_y^f = 5\mathrm{LG}_{00}^{\sigma_y} - 7\mathrm{LG}_{01}^{\sigma_y} + 40\mathrm{LG}_{02}^{\sigma_y} - 18\mathrm{LG}_{03}^{\sigma_y} - 30\mathrm{LG}_{30}^{\sigma_y}, \tag{22}$$

$$E_z^f = 8\mathrm{LG}_{00}^{\sigma_z} - 18\mathrm{LG}_{01}^{\sigma_z} + 40\mathrm{LG}_{02}^{\sigma_z} - 18\mathrm{LG}_{03}^{\sigma_z} - 34\mathrm{LG}_{30}^{\sigma_z}, \tag{23}$$

with $\sigma_y = 0.42\lambda$ and $\sigma_z = 0.5\lambda$. The formulas of equation (23) were obtained according to [27, 30], with coefficients adapted to the non-paraxial situation [1]. We filter in transverse Fourier space with H_{k_0} and H_0, where the latter is only necessary for E_z^f.

Even though at first glance the two linked vortex knots in figure 8 may seem somewhat contrived, they highlight that vortex lines in different electric field components can be chosen to be arbitrarily close without reconnecting. This is not possible for vortex lines in a single electric field component, which could be of importance when considering inscribing these vortex lines onto matter. Furthermore, such a topology demonstrates the tremendous possibilities of structured light.

The transverse electric field component E_x^f is fully determined by equation (23). Even though E_z^f and E_y^f have finite support, E_x^f is nonzero on a semi-infinite interval and thus impractical (see figure 8). Such semi-infinite field components occur when at least one of the other components integrated over the respective variable does not vanish: in our case, $\hat{E}_{y,z}^f(k_x = 0, k_y) \neq 0$. Nevertheless, this problem of impractical field components can be circumvented by simply attenuating the beam with, e.g. a sufficiently wide super-Gaussian profile, without affecting the propagation of the components of interest close to the optical axis. Additional satellite spots will appear far from the axis, but we have checked that for a super-Gaussian $\exp[-\mathbf{r}_\perp^{10}/(10\lambda)^{10}]$ those spots do not interfere with the linked vortex knots.

5. Conclusions

In this paper we have presented a systematic route to construct numerically exact vector beams. By means of a Helmholtz decomposition of the transverse electric field components in a plane transverse to the optical axis, we show that the full electromagnetic field can be generated by two scalar potentials V and W. The potential V produces 'curl-free' (in the transverse plane) fields with a nonzero longitudinal component. The potential W produces 'divergence-free' (in the transverse plane) fields with zero longitudinal component. We suggest naming these *generalized radial* and *azimuthal polarization states*, respectively. The decomposition of the optical field into generalized radial ($W = 0$) and azimuthal ($V = 0$) polarization states allows us to draw several analogies with other physical systems, that is, electrostatics, magnetostatics, and fluid dynamics. By means of these analogies, it is possible develop an intuitive understanding of the interrelation between longitudinal and transverse electric field components, and the scalar potentials assume a 'physical meaning'. Finally, we presented several examples to illustrate the proposed decomposition and analogies. Besides rather simple configurations such as longitudinal vortices, we demonstrated arbitrary random beams as well as sophisticated topological light configurations. In all these examples, the above analogies were used to explain features in the respective electric field components, or even to conceive the beam configurations.

We believe that our findings will broaden the range of accessible vector beams extensively and trigger further theoretical and experimental investigations involving structured light.

Funding Information

This work is funded by the Leverhulme Trust Research Programme Grant RP2013-K-009, SPOCK: Scientific Properties Of Complex Knots. SS acknowledges support by the Qatar National Research Fund through the National Priorities Research Program (Grant No. NPRP 8-246-1-060).

ORCID iDs

F Maucher https://orcid.org/0000-0002-5808-3967
S Skupin https://orcid.org/0000-0002-9215-1150
S A Gardiner https://orcid.org/0000-0001-5939-4612
I G Hughes https://orcid.org/0000-0001-6322-6435

References

[1] Maucher F, Skupin S, Gardiner S A and Hughes I G 2018 Creating complex optical longitudinal polarization structures *Phys. Rev. Lett.* **120** 163903
[2] Richards B and Wolf E 1959 Electromagnetic diffraction in optical systems. ii. structure of the image field in an aplanatic system *Proc. R. Soc.* A **253** 358–79
[3] Youngworth K S and Brown T G 2000 Focusing of high numerical aperture cylindrical-vector beams *Opt. Express* **7** 77
[4] Quabis S, Dorn R, Eberler M, Glöckl O and Leuchs G 2000 Focusing light to a tighter spot *Opt. Commun.* **179** 7
[5] Dorn R, Quabis S and Leuchs G 2003 Sharper focus for a radially polarized light beam *Phys. Rev. Lett.* **91** 233901
[6] Wang H, Shi L, Lukyanchuk B, Sheppard C and Chong C T 2008 Creation of a needle of longitudinally polarized light in vacuum using binary optics *Nat. Photon.* **2** 501
[7] Bauer T, Banzer P, Karimi E, Orlov S, Rubano A, Marrucci L, Santamato E, Boyd R W and Leuchs G 2015 Observation of optical polarization Möbius strips *Science* **347** 964–6
[8] Quinteiro G F, Schmidt-Kaler F and Schmiegelow C T 2017 Twisted-light-ion interaction: the role of longitudinal fields *Phys. Rev. Lett.* **119** 253203
[9] Hnatovsky C, Shvedov V, Krolikowski W and Rode A 2011 Revealing local field structure of focused ultrashort pulses *Phys. Rev. Lett.* **106** 123901
[10] Nye J F 1999 *Natural Focusing and Fine Structure of Light: Caustics and Wave Dislocations* (Bristol: Institute of Physics Publishing)
[11] Lekner J 2003 Polarization of tightly focused laser beams *J. Opt. A: Pure Appl. Opt.* **5** 6
[12] Otte E, Tekce K and Denz C 2017 Tailored intensity landscapes by tight focusing of singular vector beams *Opt. Express* **25** 20194–201
[13] Lekner J 2016 Tight focusing of light beams: a set of exact solutions *Proc. R. Soc.* A **472** 20160538
[14] Adams C S and Hughes I G 2018 *Optics f2f* (Oxford: Oxford University Press)
[15] Batchelor G K 2000 *An Introduction to Fluid Dynamics* (Cambridge: Cambridge University Press)
[16] Nieminen T A, Stilgoe A B, Heckenberg N R and Rubinsztein-Dunlop H 2008 Angular momentum of a strongly focused Gaussian beam *J. Opt. A: Pure Appl. Opt.* **10** 115005
[17] Kleckner D and Irvine W T M 2013 Creation and dynamics of knotted vortices *Nat. Phys.* **9** 253
[18] Maucher F and Sutcliffe P M 2016 Untangling knots via reaction-diffusion dynamics of vortex strings *Phys. Rev. Lett.* **116** 178101
[19] Maucher F and Sutcliffe P M 2017 Length of excitable knots *Phys. Rev.* E **96** 012218
[20] Maucher F and Sutcliffe P M 2018 Dynamics of linked filaments in excitable media arXiv:1804.07064
[21] Binysh J, Whitfield C A and Alexander G P 2019 Stable and unstable vortex knots in excitable media *Phys. Rev.* E **99** 012211
[22] Tkalec U, Ravnik M, Copar S, Zumer S and Musevic I 2011 Reconfigurable knots and links in chiral nematic colloids *Science* **333** 62–5

[23] Martinez A, Ravnik M, Lucero B, Visvanathan R, Zumer S and Smalyukh I I 2014 Mutually tangled colloidal knots and induced defect loops in nematic fields *Nat. Mater.* **13** 258–63
[24] Martinez A, Hermosillo L, Tasinkevych M and Smalyukh I I 2015 Linked topological colloids in a nematic host *Proc. Natl Acad. Sci. USA* **112** 4546–51
[25] Proment D, Onorato M and Barenghi C F 2012 Vortex knots in a Bose–Einstein condensate *Phys. Rev.* E **85** 036306
[26] Kleckner D, Kauffman L H and Irvine W T M 2016 How superfluid vortex knots untie *Nat. Phys.* **12** 650
[27] Dennis M R, King R P, Jack B, O'Holleran K and Padgett M J 2010 Isolated optical vortex knots *Nat. Phys.* **6** 121
[28] Sugic D and Dennis M R 2018 Singular knot bundle in light *J. Opt. Soc. Am.* A **35** 1987–99
[29] Ruostekoski J and Dutton Z 2005 Engineering vortex rings and systems for controlled studies of vortex interactions in Bose-Einstein condensates *Phys. Rev.* A **72** 063626
[30] Maucher F, Gardiner S A and Hughes I G 2016 Excitation of knotted vortex lines in matter waves *New J. Phys.* **18** 063016